Mechanisms of Hydrate Blockage in Oil-water Dispersions Based on Flow Loop Experiments

Vinicius R. de Almeida, Eric Serris, Gianluca Lavalle, Ana Cameirão, Jean-Michel Herri, Emilie Abadie, Nicolas Lesage, Annie Fidel-Dufour

To cite this version:

Vinicius R. de Almeida, Eric Serris, Gianluca Lavalle, Ana Cameirão, Jean-Michel Herri, et al.. Mechanisms of Hydrate Blockage in Oil-water Dispersions Based on Flow Loop Experiments. Chemical Engineering Science, 2023, 273, pp.118632. 10.1016/j.ces.2023.118632 . emse-04032496

HAL Id: emse-04032496
https://hal-emse.ccsd.cnrs.fr/emse-04032496v1

Submitted on 24 Oct 2023

Mechanisms of Hydrate Blockage in Oil-water Dispersions Based on Flow Loop Experiments

Vinicius De Almeida[1,*], Eric Serris[1], Gianluca Lavalle[1], Ana Cameirão[1], Jean-Michel Herri[1], Emilie Abadie[2], Nicolas Lesage[2], Annie Fidel Dufour[2]

[1]Mines Saint-Etienne, Univ Lyon, CNRS, UMR 5307 LGF, Centre SPIN, F – 42023 Saint-Etienne, France

[2]TotalEnergies, CSTJF, Avenue Larribau, Pau Cédex 64018, France

*Corresponding author: vinicius.de-almeida@emse.fr (V. De Almeida)

Abstract: Hydrate formation poses a threat to the safety of petroleum transport in flow lines due to the risk of plugging. In this work, conceptual mechanisms of hydrate formation and plugging in oil-water systems are proposed, based on flow loop tests at 30%, 50% and 80% water cut (water fraction). The experiments were conducted using Kerdane oil, water (with 30 g/L of NaCl) and natural gas at 75 bar and 4 °C. The employment of several instruments, such as acoustic emission, permittivity, and flowmeter, to cite a few, allowed identifying the different flow patterns until hydrate blockage and detecting the phase that carries the hydrates. A model based on density measurement is proposed to calculate the fraction of hydrates flowing locally. It was observed that there are local accumulations of most of the hydrates in a small portion of the flowing volume, which, together with deposition, ends up leading to plugging.

Keywords: flow assurance, petroleum flowlines, hydrate formation, mechanisms of plugging, flow loop experiments, oil-water dispersions.

1 Introduction

The operational safety and economical regards involving multiphase flow transport in petroleum flowlines are studied in an engineering analysis process called flow assurance. Flow assurance's most important issues are the appearance and deposition of solids in deepwater long-distance flow lines due to the high pressures and low temperatures (Olajire, 2020). In case of pipeline blockage, the operation must be interrupted for remediation, risking the occurrence of accidents and financial losses. Among the flow assurance issues, hydrate problems might be the most significant challenge nowadays (Cardoso et al., 2015; Jamaluddin et al., 1991; Sloan and Koh, 2008).

Gas hydrates are crystalline compounds formed from a network of hydrogen-bonded water molecules entrapping light natural gas molecules (Englezos, 1993; Khurana et al., 2017). These crystals are studied in different applications, including, for example, their use as an energy source (Shaibu et al., 2021). In the oil and gas industry, hydrates form when the undesired water content in flow lines is in interaction with gas under high pressure and low temperature (Sloan, 2003; Sum et al., 2009). Gas hydrates have a dual effect on multiphase flow: (i) they change the characteristics of the slurry flow and the flow pattern (Delahaye et al., 2008; Ding et al., 2016); (ii) the particles may agglomerate or form deposits (Bassani et al., 2017; Chen et al., 2014; Stoner and Koh, 2021; Straume et al., 2016; Wang et al., 2020) due to the capillary forces (Colombel et al., 2009), which affect the rheological properties (Chen et al., 2022; Ding et al., 2019; Fidel-Dufour et al., 2006; Liu et al., 2020; Pham et al., 2020; Sinquin et al., 2004; Song et al., 2019), possibly leading to the onset of plugging.

The formation of gas hydrates in oil-water systems has been the object of many research. The first studies proposed that hydrates form a shell around water droplets in water-in-oil systems with an inward growth (Melchuna et al., 2016; Sloan et al., 2011; Turner, 2005), or a shell around oil droplets in oil-in-water systems that has an outward growth (Melchuna et al., 2016; Sloan et al., 2011). The models assume that hydrate formation occurs at the oil-water interfaces, as the gas is mainly dissolved in the oil phase. As a result, for the shell approach, hydrates always entrap the dispersed phase. As an alternative to the shell approach, a “sponge approach” has been recently proposed, where hydrates are porous structures that entrap only the water phase (Bassani et al., 2019). While most of the data available in the literature are limited to oil continuous systems, there is an increasing demand for water continuous test cases. Indeed, in order to maintain a petroleum reservoir explorable, the pressure must be kept constant, and this is done by means of continuous water injection.

A unified hydrate formation flow model for different flow characteristics (oil-dominated, gas-dominated, gas condensate, and high water cut system) does not exist. Identifying which phase, oil or water, transports hydrates at different conditions could help to better understand hydrate blockage. The literature has not yet reported a methodology that allows this analysis. Although agglomeration and deposition have commonly been considered the dominant mechanisms of plugging, it is possible that changes in the multiphase flow due to hydrate formation may play an important role in hydrate blockage risk. While solid agglomeration and multiphase flow are often studied separately, an analysis combining these two is necessary for addressing this costly flow assurance problem in offshore petroleum exploration.

In this sense, the objective of this work is to present new insights about the two-way coupling between flow regime and hydrate formation. This paper aims to answer the following questions: (i) How do different oil-water systems affect hydrate formation? (ii) How do hydrates act on the flow pattern and on the flow characteristics? (iii) How do hydrate plugs form? To answer these questions, flow loop experiments were conducted to study the different stages of hydrate slurry formation and plugging at low, intermediate, and high water cuts. The facility is equipped with a unique combination of instruments that allows detecting the continuous phase, tracking hydrate particles, and detect which phase carries the hydrates. The impact of hydrate formation on multiphase flow and the main cause of plugging for each scenario are discussed. An extensive analysis is carried out in order to identify the flow regime at each different stage of the tests. A simplified model using the density measured by a flowmeter is proposed to calculate the local accumulations of hydrates in the flow. Finally, based on this model, a methodology is proposed to classify the different tests according to their heterogeneity in hydrate distribution along the pipe.

2 Experimental methodology

2.1 Flow loop description

The Archimede flow loop, illustrated in Figure 1, consists of a pipeline that is approximately 56 meters long, divided into three sections: a vertical downward section, a slightly inclined or horizontal section, and a vertical upward section. The vertical sections have a pipe internal diameter of 15.7 mm, while the slightly inclined or horizontal section has a pipe internal diameter of 10.2 mm. The temperature is controlled by a cooling system composed of two circulating baths (one for the horizontal section and the other for the vertical sections), which send a refrigerated fluid (mixture of water and ethanol) to the heat exchanger pipes. In order to limit heat exchange with the room, the entire flow loop apparatus is jacketed with an insulating material. A Moineau pump, which allows a flow rate of up to 500 L/h, provides the power for the circulation of the liquid in the pipeline.

The flow loop is equipped with several probes, listed in Table 1, that measure temperature, absolute pressure, pressure drops, the gas flow rate injected by an automatic gas compensation system, density, and flow rate (monitored by means of a Coriolis flowmeter). Furthermore, the apparatus is equipped with a high-speed camera (HSC), a Particle Vision Microscope (PVM), a Focused Beam Reflectance Measurement (FBRM), an acoustic emission technology system (AE) and a permittivity probe.

Table 1. Probes installed in the Archimede flow loop, with their notations and features.

Instrument	**Notation / Measurements**	**Feature**

Temperature probes	T_1-T_{10}	Nine equally distributed sensors along the loop and one additional for room temperature. Measurements in °C every 1.0 s.
Pressure probe	p_{abs}	Absolute pressure of the gas in the separator. Measurements in bar every 1.0 s.
Pressure drops probes	Δp_1, Δp_2, Δp_4, Δp_h	Pressure drops at the downward and upward vertical sections (Δp_1 and Δp_2, in bar), gravitation pressure drop on the right vertical pipe of the separator (Δp_4, in mbar), and horizontal section (Δp_h, in bar). Measurements every 1.0 s.
Coriolis flowmeter (density and flow rate)	ρ, Q	Measures the density (in kg/m^3) and the flow rate (in L/h) at the downward section. Measurements every 1.0 s.
Gas injection	p_c, Q_G	Automatic gas compensation system with an absolute pressure and a gas flow meter probe. Measurements in NL/min every 1.0 s.
Acoustic emission	AE	Measures the absolute energy (in aJ) every 0.5 s. using 4 or 6 sensors, as shown in Figure 1, identified as 1A to 4A (in blue) or from 1B to 6B (in red).
Focused beam reflectance measurement	FBRM	Measures chord counts (per second) in a 1-1000 µm range every 5.0 s.
Particle vision measurement	PVM	Microscope coupled with a camera that takes pictures of the flow at a resolution of 1050 x 825 µm every 5.0 s.
Permittivity probe	ε_r	It measures the relative permittivity near the wall every 3 to 6 s.
High-speed camera	HSC	Monochromatic camera installed in front of a 52 x 12 mm visualization window. Up to 1GB/s or 211 fps at a maximum resolution of 2560 x 2048 pixels.

Pipeline length	Horizontal: 36.0 m Upward: 10.5 m Downward: 9.5 m
Pipeline diameter	Horizontal: 10.2 mm Verticals: 15.7 mm
Moineau pump	100 - 500 L/h
Volume	13.3 L liquid: 10.0 L gas: 3.3 L
Pressure	75 bar
Temperature	4 °C

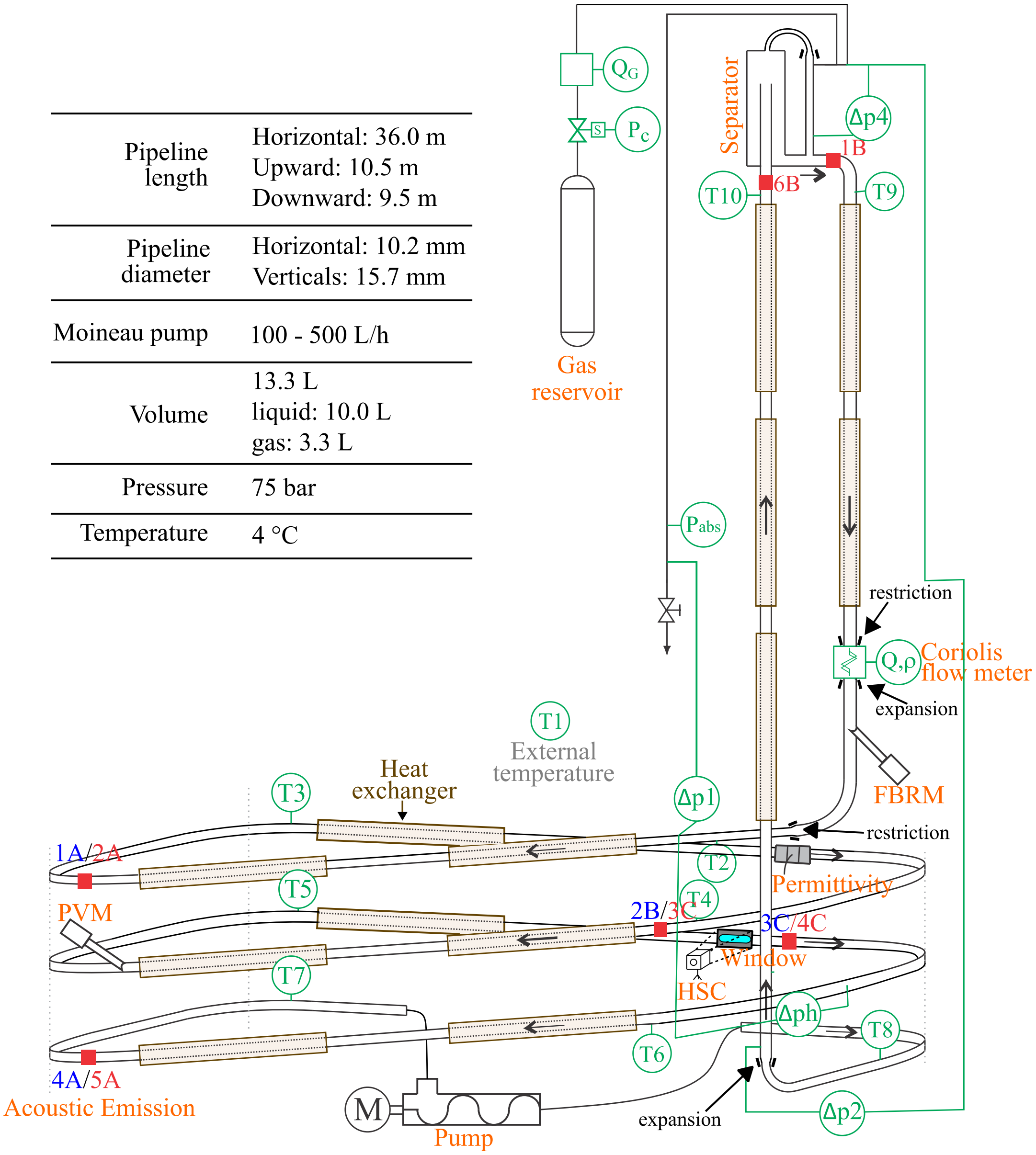

Figure 1. Schematic illustration of the Archimède flow loop.

2.2 Experimental conditions and protocol

The experiments are conducted with oil, saline water and natural gas. Table 2 specifies the physical properties of the fluids at room pressure and temperature, while Table 3 provides the composition of the natural gas. Table 4 specifies the control parameters according to their variation range. Each experimental condition, defined by a combination of water cut and flow rate, was repeated at least once.

Table 2. Fluids used for the experiments and their properties.

Fluid	Description	Fluid properties
Salted water	30 g of NaCl per L of deionized water.	Density: 1023.8 g/L Viscosity: 0.0026 Pa.s
Kerdane oil	Hydrocarbons, C11-C14, n-alkanes, isoalkanes, cyclics, <2% aromatics.	Density: 815 g/L Viscosity: 0.0017 Pa.s

Table 3. Composition of the natural gas.

Gas	%mol
Methane	91.7
Ethane	5.9
Propane	0.6
Carbon dioxide	0.8
Nitrogen	0.8
i-butane	0.1
n-butane	0.1

Table 4. Control parameters for the experiments.

Parameter	Values
Flow rate	200 L/h, 400 L/h
Water cut	30%, 50%, 80%

The experimental protocol, illustrated in Figure 2, can be summarized in four main steps:

i. Controlling the flow rate at 200 or 400 L/h.
ii. Cooling down the temperature to a minimum of 4 °C.
iii. Fast pressurizing to 75 bar.
iv. Maintaining the pressure constant by means of the gas compensation system.

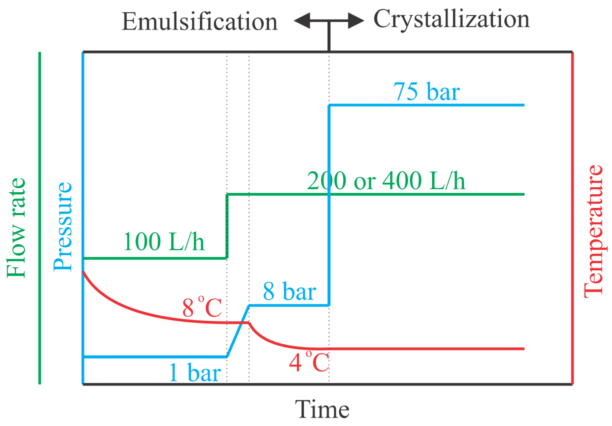

Figure 2. Experimental protocol.

During the last step (iv), the injected gas flow rate is measured in order to calculate the amount of gas consumed for hydrate formation. Some intermediate steps (flow rate control to 100 L/h, temperature to 8 °C and absolute pressure to 8 bar) are applied in order to reduce the influence of room temperature on the results during emulsification, as shown in Figure 2.

2.3 Data synchronization

Due to the many instruments that are installed in the flow loop, where each one of them is placed in a different position, a methodology to synchronize the data was developed. In order to compare the same portion of the flow when it passes in front of two different instruments, the time required for the flow to move from one of the instruments to the other is calculated. This calculation is a function of the volume between the instruments and the flow rate measured by the Coriolis flowmeter. When this time correction is applied, an indication is given on the x-axis of the graphs (see, for instance, Figure 5). The procedure applied for this paper consisted of fixing the flowmeter as a reference and then correcting the time data set of the other instruments in a way to synchronize them with the time data sets obtained with the flowmeter.

3 Methodology to calculate the hydrate volume

With the aim to determine the hydrate fraction and the water conversion as a function of time, a model based on mass and volume balances is proposed. The model has the following assumptions:

- The mass of gas dissolved in the oil phase is constant after the onset of hydrate formation.

- The fraction of each gas component being consumed for hydrate formation is proportional to its mole fraction in the free gas.
- The hydrate density is constant and equal to 910 g/L, which is approximately the density of methane hydrates (Sloan and Koh, 2008).
- The hydration number, that is, the ratio between the number of water molecules and gas molecules consumed for hydrate formation, is constant and equal to 6.0.

The mass balance, considering the mass of free gas (m_G), the mass of free water (m_W) and the mass of hydrates (m_H), is given by the following equation:

$$m_G + m_W + m_H = m_G^0 + m_W^0 + m_{G,inj} \tag{1}$$

where the superscript 0 corresponds to the instant of onset of hydrate formation. The term $m_{G,inj}$ is the mass of gas injected by the gas compensation system since the onset of hydrate formation. The volume balance between gas volume (V_G), water volume (V_W) and hydrate volume (V_H) is represented by the following equation:

$$V_G + V_W + V_H = V_G^0 + V_W^0 \tag{2}$$

One should notice that the oil phase and the dissolved gas were not considered in equations (1) and (2). This is because the oil mass is constant over time, and the amount of dissolved gas is assumed to be constant after the onset of hydrate formation. The gas density can be calculated from the pressure, temperature and composition of the gas using the Soave–Redlich–Kwong equation of state, and can be used to relate the mass and volume of the gas:

$$\rho_G(p,T) = \frac{m_G}{V_G} \tag{3}$$

As previously mentioned, hydrate density is assumed to remain constant at 910 g/L, and it is the ratio between hydrate's mass and volume:

$$\rho_H = \frac{m_H}{V_H} \tag{4}$$

The water density is also constant and given by:

$$\rho_W = \frac{m_W}{V_W} \tag{5}$$

Finally, the hydration number is:

$$N_h = \frac{(m_{\mathrm{W}}^0 - m_W)\Big/ M_{\mathrm{W}}}{\left(m_{\mathrm{G}}^0 + m_{G,inj} - m_G\right)\Big/ M_{\mathrm{G}}} \tag{6}$$

where M_W is the water molar mass and M_G is the gas molar mass. Substituting the equations (3)-(5) into equation (1), and then combining them with equations (2) and (6), we obtain the following system of equations, where V_w, V_G and V_H are the unknowns to be determined:

$$\begin{bmatrix} \rho_W & \rho_G & \rho_H \\ 1 & 1 & 1 \\ \dfrac{\rho_W}{M_W} & -\dfrac{N_h \rho_G}{M_G} & 0 \end{bmatrix} \begin{bmatrix} V_W \\ V_G \\ V_H \end{bmatrix} = \begin{bmatrix} m_G^0 + m_{G,inj} + m_W^0 \\ V_G^0 + V_W^0 \\ \dfrac{m_W^0}{M_W} - N_h \left(\dfrac{m_G^0 + m_{G,inj}}{M_G} \right) \end{bmatrix} \tag{7}$$

Once the volume of each phase is known, it is possible to calculate the global hydrate fraction in the system relatively to the oil and water phases, which are the phases that circulate in the loop with the hydrates. The hydrate fraction is given by the following expression:

$$\alpha_H = \frac{V_H}{V_H + V_W + V_O} \tag{8}$$

where V_O is the oil volume, which is constant.

4 Results and discussion

The results of the carried-out experiments, summarized in Table 5, are discussed in six subsections. In the first one, it is introduced the methodology for identifying the continuous phase for characterizing the flow pattern before hydrate formation. The subsequent three subsections present the results of hydrate formation for tests at low, intermediate and high water cut. The fifth subsection presents a methodology to quantify the local hydrate fraction and to characterize the heterogeneity of the system. The last subsection presents a summary of the main outcomes.

Table 5. List of experiments.

Experiment	Water cut	Flow rate	Water conversion	Hydrate fraction	Time with hydrates until plug
#1	30%	200 L/h	18.7%	8.0%	13.4 min
#2			11.1%	4.1%	6.1 min

#3		400 L/h	13.2%	4.9%	3.2 min
#4			9.6%	3.6%	3.8 min
#5	50%	200 L/h	3.7%	2.4%	6.6 min
#6			2.2%	1.4%	3.9 min
#7			2.9%	1.8%	4.7 min
#8			4.6%	2.9%	5.8 min
#9		400 L/h	10.6%	6.6%	7.3 min
#10			18.5%	11.7%	13.7 min
#11			14.6%	9.2%	9.3 min
#12	80%	200 L/h	7.8%	8.0%	92.1 min
#13			10.3%	10.6%	120.1 min
#14		400 L/h	11.7%	11.9%	26.9 min
#15			16.3%	16.4%	37.3 min

4.1 Permittivity measurements to identify the continuous phase

Identifying the continuous phase and whether the dispersed system is oil-in-water or water-in-oil before hydrate formation is important because hydrates preferentially form at oil-water interfaces, and thus their shape, kinetics and dynamics are strongly affected by the two-phase flow pattern. In this work, a combination of the following three measurements is used to identify the dispersed phase before hydrate formation: the dielectric, the local water fraction calculated from the density, and the images from the camera.

The dielectric of saline water with 30 g NaCl/L is 87.9, while the dielectric of the Kerdane oil is 2.7, both at 4 °C, values obtained from tests in the flow loop apparatus. The local or instantaneous water fraction ($\alpha_{l,W}$) that passes through the flowmeter is calculated from the measured density (ρ), using the equation:

$$\rho = \rho_W \alpha_{l,W} + \rho_O (1 - \alpha_{l,W}) \tag{9}$$

where ρ_W and ρ_O are the densities of water and oil.

In order to obtain the dielectric as a function of the water fraction, an algorithm is proposed, as illustrated in Figure 3. In every 30-second slot of the whole measurement, the highest, lowest and time-averaged values of dielectric are calculated, as depicted in Figure 3(a). The same procedure is performed for the calculated water fraction, as represented in Figure 3(b). These values of dielectric and water fraction are synchronized in such a way that, for each interval of 30 seconds, the highest value of dielectric is coupled with the highest value of the water fraction, the same for their respective average and lowest values, as shown in Figure 3(c). This method is applied to the entire dataset before hydrate formation.

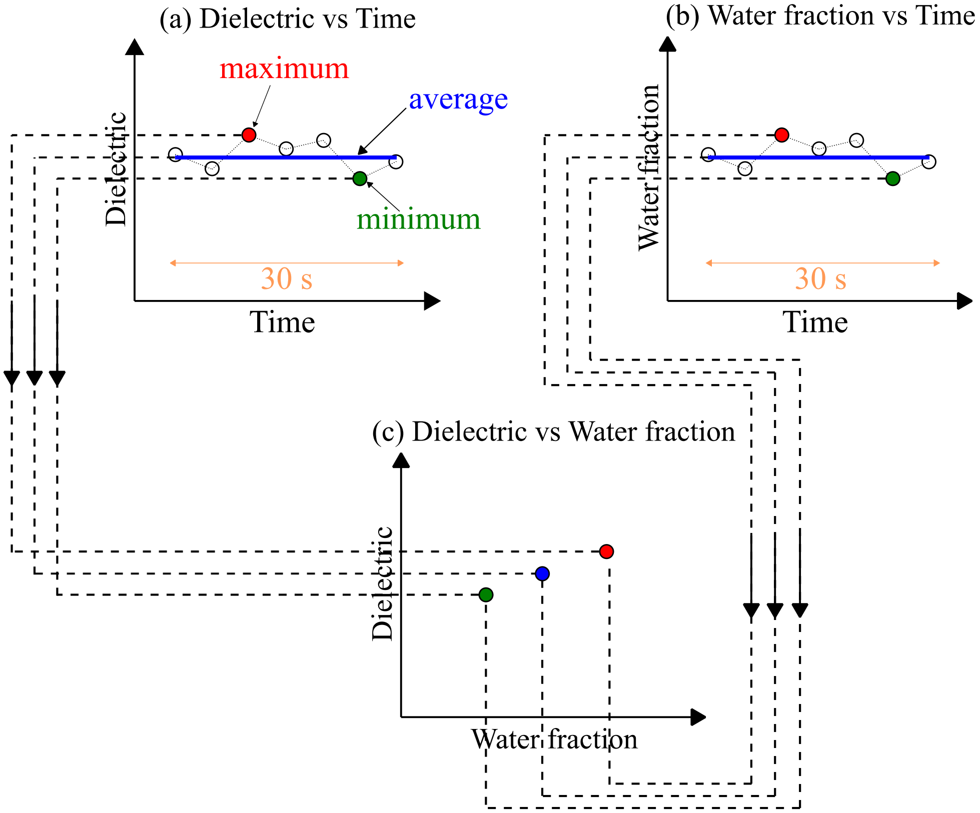

Figure 3. Representation of the algorithm to obtain the dielectric as a function of the water fraction.

The proposed method allows obtaining a dataset (dielectric vs. water fraction) that helps to identify the dispersed phase. Validation of the results is achieved by comparison with camera images in Figure 4. At 200 L/h the dispersions are not completely homogeneous. At 30% water cut and 200 L/h, the water fraction can vary locally from 15% to over 50% (Figure 4(a)). For a test at 50% water cut and 200 L/h, the local water fraction can range from 20% to 80% (Figure 4(c)). This heterogeneity can be clearly observed in the images from the camera, showing the presence of droplets whose size covers several millimeters. As the flow rate increases, at 400 L/h, the heterogeneity reduces because the higher shear rate breaks the droplets. This can be observed in the images, which show a thinner dispersion than at 200 L/h, confirmed by our measured dielectric and calculated water fractions, which show a shorter range (see Figure 4(b,d,f)).

The results also show that there is a direct relation between the local water fraction and the dielectric, with the dielectric increasing as the water fraction increases. At 30% water cut, oil has been identified as the continuous phase. At 200 L/h, this is highlighted in the images from the camera (Figure 4(a)) that water droplets are dispersed in the oil continuous phase (bright droplets dispersed in the dark background), whereas at 400 L/h (Figure 4(b)) the dielectric values are much closer to the oil dielectric than to the water dielectric. At 50% and 80% water cut, water has been identified as the continuous phase as the dielectric values are much closer to the water dielectric than to the oil dielectric (Figure 4(c-f)). Also, images from the camera show that oil droplets, which are lighter and concentrated preferably at the top of the window due to gravity, are dispersed in the water continuous phase.

(a) 30% water cut, 200 L/h

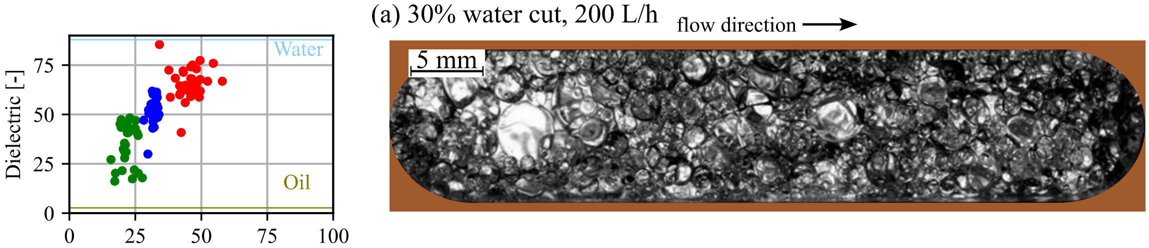

(b) 30% water cut, 400 L/h

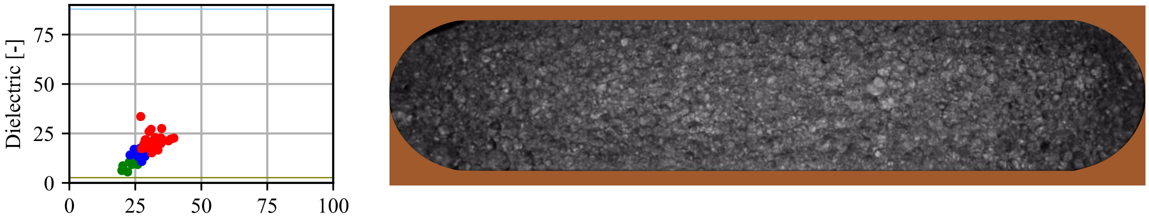

(c) 50% water cut, 200 L/h

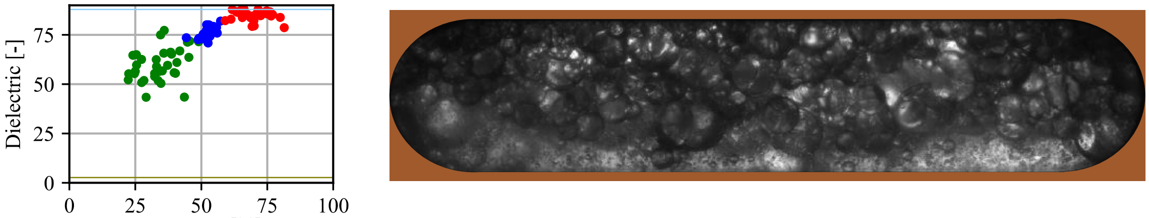

(d) 50% water cut, 400 L/h

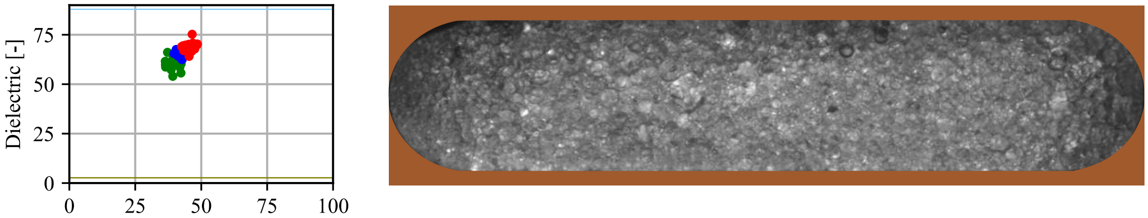

(e) 80% water cut, 200 L/h

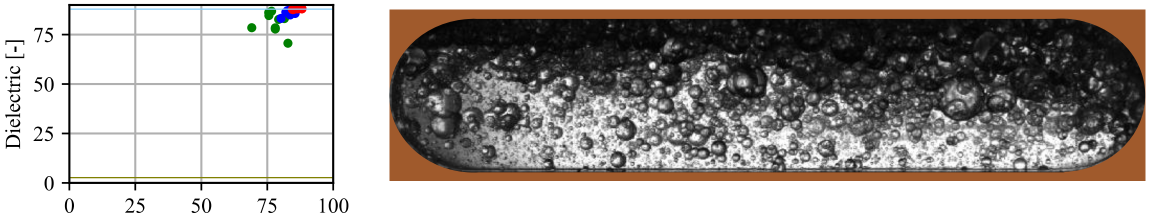

(f) 80% water cut, 400 L/h

Figure 4. Analysis of the flow regime comparing dielectric vs. water cut (left panels) to images obtained from the camera (right panels) as a function of water cut and flow rate.

4.2 Hydrate formation at low water cut

Figure 5 shows the time evolution of dielectric and density (top panel), of dielectric and absolute energy for the sensor 1A (central panel), and of pressure drops and flow rate (bottom panel) for a test conducted at 30% water cut and 200 L/h. Hydrate formation was detected after 17.5 minutes, as evidenced by the sudden decrease in density and dielectric at that time (Figure 5(a)). The decrease in density and dielectric is attributed to the reduction in water fraction as water is consumed for hydrate formation. From the onset of hydrate formation (at 17.5 minutes) to hydrate blockage (at 30.0 minutes, when the experiment ends), the flow had different stages. Initially, during the first three minutes, the particles were dispersed everywhere in the flow, as can be deduced from the absolute energy (Figure 5(b)), which significantly increased and remained at high values for three minutes. High values of absolute energy are indicators of hydrate transit and low values correspond to the same level prior to the formation of hydrates (de Almeida et al., 2022). However, at 20.5 minutes, the flow regime began exhibiting intermittent behavior, with some parts of the flow transporting hydrates (peaks of absolute energy) and others containing only liquid. As the absolute energy peaks were mostly in phase with the peaks of density and dielectric (Figure 5(a)), which in turn correspond to the water-governed flow, it is concluded that the hydrate particles are transported by the water phase. On the other hand, the troughs of absolute energy correspond to the oil-governed flow, as they were mostly in phase with the troughs of dielectric (Figure 5(b)) and density (Figure 6).

During the first three minutes after hydrate formation, as the particles were evenly dispersed in the liquid, the horizontal pressure drop increases significantly (blue line in Figure 5(c)). This increase in pressure drop is believed to be due to an increase in apparent viscosity that occurs as more interfaces are created when hydrates form. However, as the flow starts to became more heterogeneous, at 20.5 minutes, the horizontal pressure drop reduced, due to a reduction of the interfacial area between the phases. Meanwhile, the local accumulation of hydrates in parts of the pipeline started to cause significant restrictions. This can be noted, for instance, from the pressure drop in the right vertical pipe of the separator (Δp_4, cyan line in Figure 5(c)), which reduced when hydrates passed through the separator. This indicates that, when hydrates pass therein, they cause a restriction at the bottom of the separator that temporarily interrupts the flow. This causes the suction of liquid from the right vertical pipe of the separator, explaining why the liquid level in that part of the separator reduced. The hydrate plugging was observed after 30 minutes, when the flow rate indicated zero, causing the end of the experiment. It was therefore a sudden event and was caused by a restriction in the bottom pipeline of the separator.

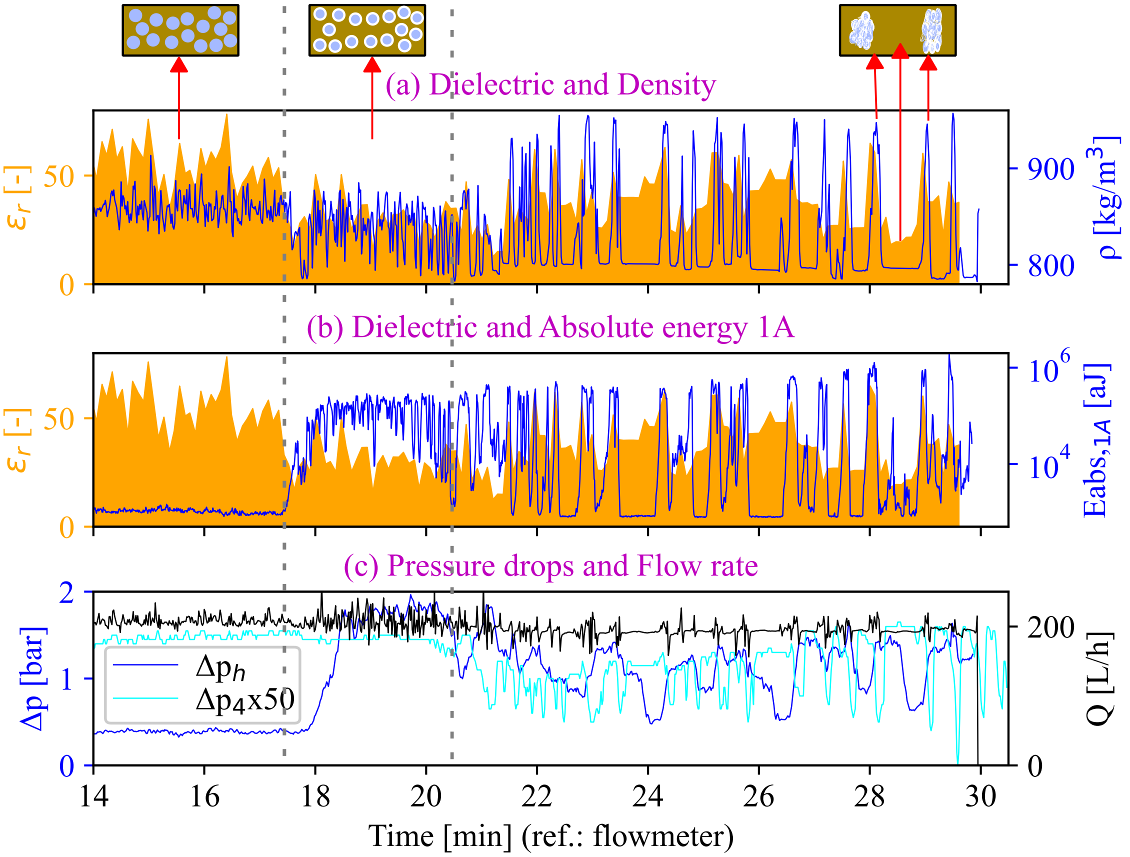

Figure 5. Experiment at 30% water-cut and 200 L/h (#1 in Table 5), showing the time evolution of (a) dielectric and density, (b) dielectric and absolute energy, and (c) pressure drops and flow rate.

The visual observation that peaks of density and absolute energy (shown in Figure 5) are in phase, which indicates that hydrates are carried by the water phase, can be verified statistically by using a time-lagged cross-correlation (Cheong, 2020). This gives the time synchrony between two data sets and consists in incrementally shifting one data set over time and repeatedly calculating the correlation to the other data set. If the peak correlation is at the center (no time lag), this indicates the signals are mostly in-phase at that time interval. To obtain the correlation between two signals, the Pearson correlation can be used (Schober and Schwarte, 2018). This is a correlation coefficient that ranges from -1 to +1, where a coefficient +1 means that all values from one data set increase as the values from the other one increase in a perfectly linear relationship, while a coefficient -1 means that all values from one data set decrease as the values from the other one increase, also in a linear relationship. A coefficient of zero means that there is no relationship between the data sets.

Figure 6 shows a comparison between density and absolute energy (sensor 1A) at the top panel (the last six minutes of the experiment), and the correlation coefficient between these two data sets for a period of three minutes at the bottom panel. The peak for the correlation coefficient occurs near the center, for a time lag of 4 seconds, which is very low compared to the period it takes for the flow to circulate around the loop. This proves that these signals are in phase.

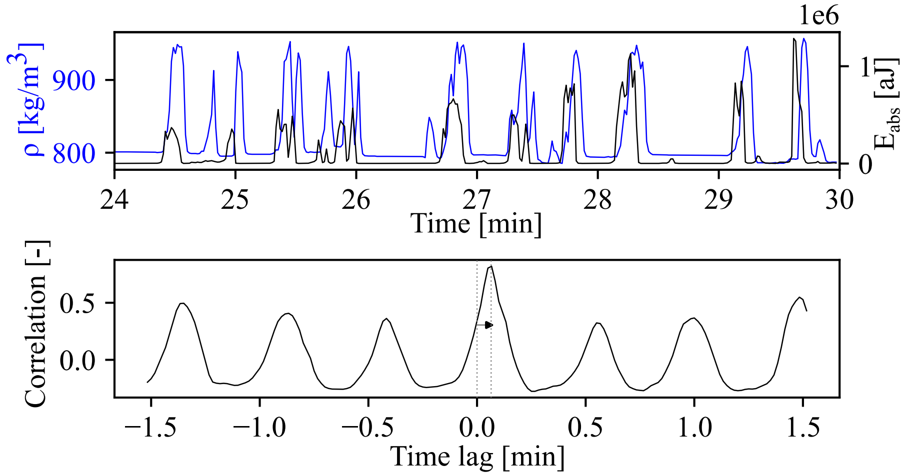

Figure 6. Time-lagged cross-correlation analysis between density and absolute energy (sensor 1A) for a test at 30% water cut (#1 in Table 5).

Hydrate formation could be detected by the images from the PVM. It is shown in Figure 7 three images: the first one was taken before hydrate formation, the second one was obtained immediately after hydrate formation, and the third one at the end of the test, just before hydrate blockage. It is shown in the first image (Figure 7(a)) a droplet with a perfectly spherical shape, most likely a water droplet dispersed in oil. Once hydrates form, as shown in Figure 7(b-c), they have an irregular shape and the appearance of a porous structure rather than solids with well-defined surfaces.

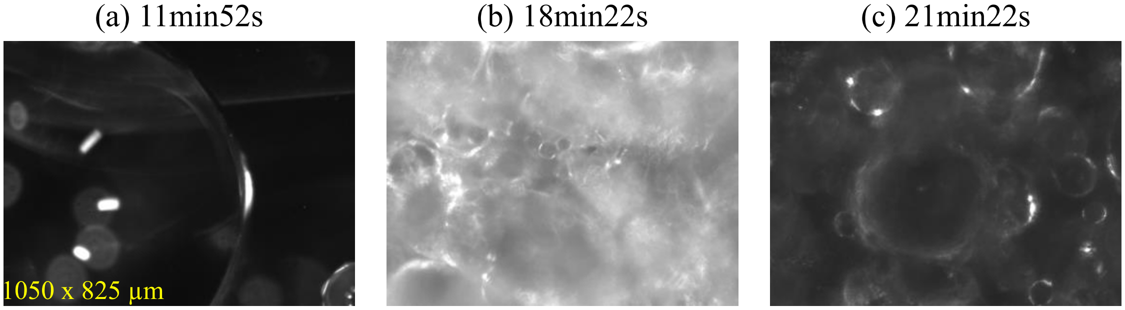

Figure 7. PVM images for the test at 30% water-cut and 200 L/h (#1 in Table 5).

Three additional tests were performed at 30% water cut, as listed in Table 5, with similar results being observed. The induction time, that is, the time required for the onset of hydrate formation, varied between 14.5 and 24.6 minutes. For all the tests, water was the carrier phase for hydrates. Furthermore, it was observed that plugging at 400 L/h occurs faster than at 200 L/h despite less water conversion. This can be explained by considering that at a higher flow rate, the flow is more homogeneous (see, for instance, Figure 4). Therefore, when hydrates form, the appearance of more interfaces between the phases is expected to increase the apparent viscosity and, as a result, the transportability of the system is reduced.

When summarizing the results from the test at 30% water cut, the most important outcomes are:

- The flow is initially water-in-oil before hydrate formation, as explained in section 4.1 by analyzing the permittivity data and images from the camera.
- During the onset of hydrate formation, hydrates are homogeneously distributed during the first few minutes, as can be deduced from the absolute energy in Figure 5(b), which consistently remains at high values for three minutes after the onset. The horizontal pressure drop (Figure 5(c)) has its highest values during this early stage of hydrate formation, as there are more interfaces between the phases and shear due to flow if the system is homogeneous. Ding et al., 2019 observed similar behavior, with the apparent viscosity being higher immediately after hydrate formation than during the stages of agglomeration, growth, and deposition.
- Water droplets rapidly coalesce, forming large pockets of sponge structures (seen in the PVM images, Figure 7) formed by water and hydrates. This was observed by synchronizing and comparing the peaks of dielectric, density and absolute energy in Figure 5(a-b), after 20 minutes. Images from the camera, shown in the top panel of Figure 8, also captured an intermittence, with the images becoming darker after hydrate formation (central image) and later presenting an intermittence (two images on the right) between parts of the flow whose images are transparent

(mostly with oil) and parts that are dark (due to the presence of hydrates, which block the lighting positioned behind the visualization window). The reason why hydrates stay preferably with the water phase can be due to the higher affinity between hydrates and water than between hydrates and oil (Bassani et al., 2019).

- A complete separation into two phases, oil and water with hydrates, is observed. The presence of large pockets of this porous structure containing hydrates and water may easily cause plugging, especially during transit towards points of singularity, where deposition or local accumulation of hydrates increases over time.

Based on test results at 30% water cut, a conceptual model for hydrate formation and plugging at low water cut in oil-water dispersed systems is proposed, shown in Figure 8. The model consists of four stages. The first stage is the entrainment of water droplets into the oil phase due to the shear caused by the flow. The second stage is the formation of hydrates on the surfaces of water droplets. As hydrates form, they eventually break down inside the water droplets. In the third stage, the water droplets with hydrates become porous structures that may easily adhere to the wall, cause some deposition, and they quickly coalesce to form large pockets of water that carry the hydrate particles. In the final stage, as the pockets of water with hydrates continue to grow, they eventually plug the pipeline. Plugging is a sudden event, and it occurs when porous-structured pockets containing water and hydrates are large enough to block the pipe.

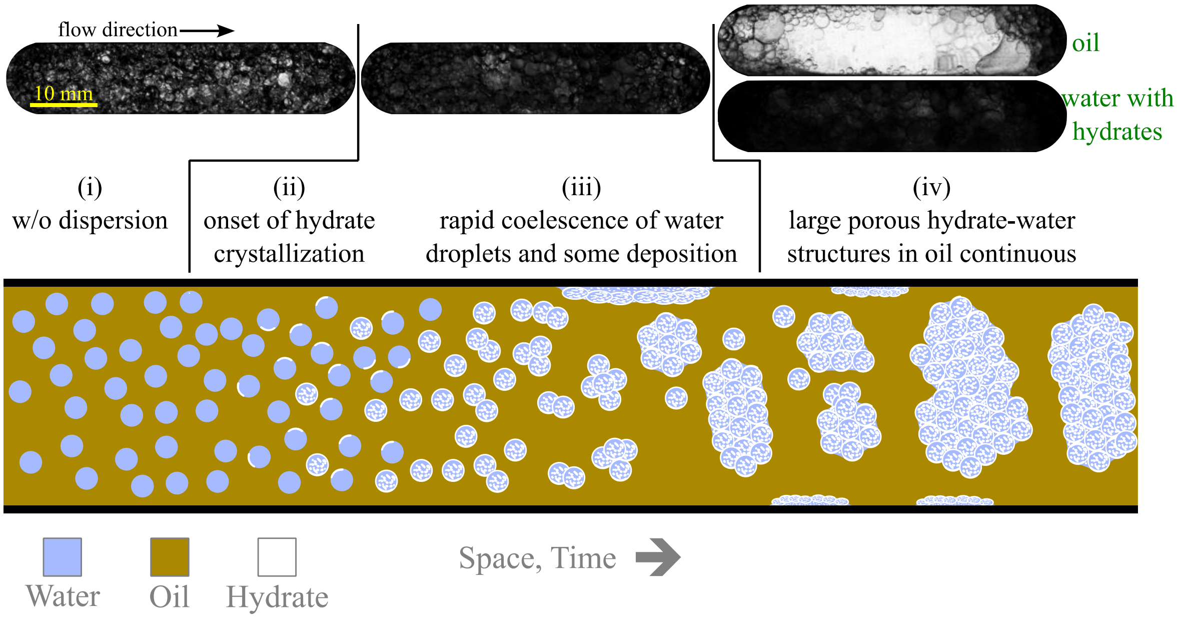

Figure 8. Depiction of the conceptual model for hydrate blockage at low water cut.

4.3 Hydrate formation at intermediate water cut

Similar to the previous section, Figure 9 shows the time evolution of dielectric and density (top panel), dielectric and absolute energy (second panel), dielectric and chord counts (third panel), and pressure drops and flow rate (bottom panel). Hydrates formed around 7 minutes, when there was a sudden reduction in dielectric and density (Figure 9(a)) along with a net increase in absolute energy (Figure 9(b)). An intermittent behavior was observed after hydrate formation, with some parts of the flow containing more oil (low density and dielectric) than others. For this test, it was also observed that it was the water phase that transported the hydrates, since regions of high density and dielectric (which contain more water) had the highest values of absolute energy. This is clear by noting in Figure 9(b) that the troughs of dielectric and absolute energy were in phase. Hydrate formation was also detected by the FBRM during the last stage of the experiment, after 12 minutes, when the flow is intermittent. It is possible to see in Figure 9(c) that the chord counts increased and showed similar oscillatory behavior to the dielectric, density and absolute energy, which confirms the presence of more particles and droplets in the part of the flow that contains more water.

There was also a temporal oscillation in the horizontal pressure drop, which is periodic and whose amplitude increases with time (Figure 9(d)). The portion of the flow that contains an accumulation of hydrates is expected to have a local apparent viscosity that increases over time and causes the blockage of the pipe. Plugging probably occurred in the downward section, as the pressure drop in this section (Δp_1) decreased whenever the hydrates passed through it and reached zero at the end of the experiment. This occurs because an increase in pressure loss due to viscosity or deposition counterbalances the gravitational differential pressure (positive for downward flow).

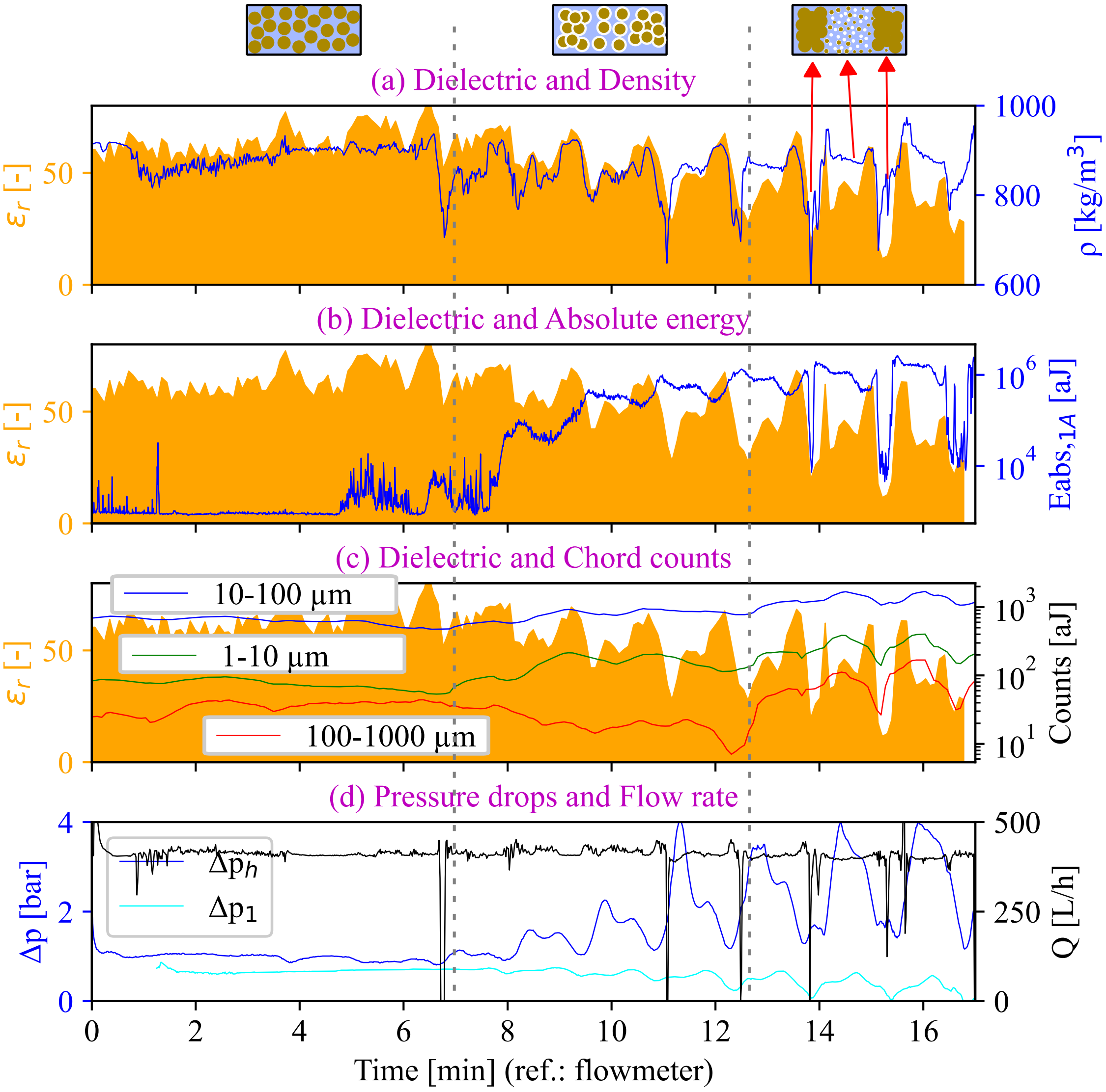

Figure 9. Experiment at 50% water-cut and 400 L/h (#10 in Table 5), showing (a) dielectric and density, (b) dielectric and absolute energy, (c) dielectric and chord counts, and (d) pressure drops and flow rate.

For the tests at 50% water cut, hydrate particles have a regular shape, and seem to be solid structures, as observed in the PVM images. Figure 10(a) shows a PVM image before hydrate formation with oil droplets of regular spherical shape. Once hydrates form, as shown in Figure 10(b-c), hydrate particles also have a regular spherical shape, indicating that these particles are entrapping oil droplets.

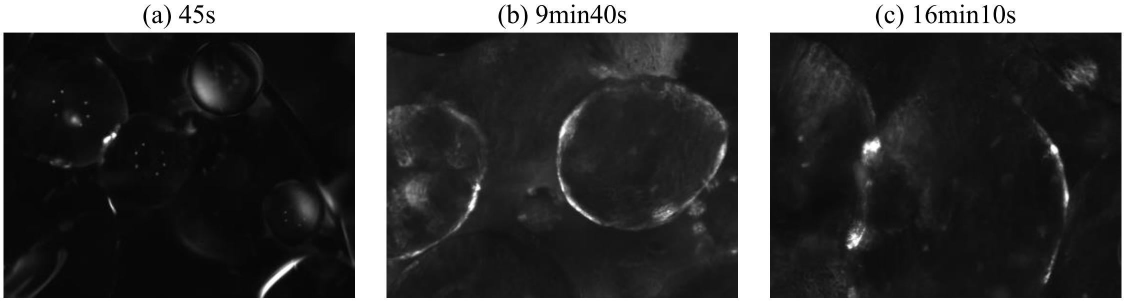

Figure 10. PVM images for a test at 50% water-cut and 400 L/h (#10 in Table 5).

A total of seven tests were conducted at 50% water cut, three of which were conducted at 200 L/h and four of which were conducted at 400 L/h. The main outcomes from these tests are:

- An oil-in-water dispersed system is the flow regime before hydrate formation, as shown in section 4.1.
- The initial oil-in-water dispersion is completely disrupted after hydrate formation. This is because the hydrates, that formed on the surfaces of oil droplets, have more affinity to the water phase. Therefore, they are detached from the oil and preferentially carried by the water phase. The conclusion that hydrates are carried by the water phase is based on the correspondence between the density, dielectric, absolute energy and chord counts measurements, whose peaks are in phase, as shown in Figure 9(a-c).
- A separation of phases occurs, with oil droplets coalescing and forming large oil pockets, while hydrates flow suspended in the water phase. This heterogeneous behavior causes an increase in pressure loss in the region of the flow that contains more hydrates. This can be observed in Figure 9(d) due to the increase in horizontal pressure drop (blue line) as hydrates pass through the horizontal section.
- Hydrates apparently entrap part of the oil droplets that are dispersed in the water phase, as seen in the PVM images (Figure 10) where there are particles with a regular shape.
- An intermittent flow forms, characterized by two regions: one containing only oil, and another containing porous hydrate structures that entrap more and more the water phase, and hydrates entrapping oil as well, increasing the pressure loss due to viscosity in these regions. The main cause of plugging was due to a blockage of hydrates in specific parts of the loop, particularly in the downward section, as shown in Figure 9(d) where the pressure drop in the downward section

(cyan line) going to zero as hydrates pass through it just before plugging, when the flow rate indicates zero as well.

Based on the results of tests at 50% water cut, a conceptual model is proposed for oil-water dispersed systems at intermediate water cut. The model in four stages is illustrated in Figure 11. The first stage consists of the entrainment of oil droplets into the water phase due to the shear caused by the flow. The second stage is the beginning of hydrate formation around oil droplets. In the third stage, the presence of hydrates causes the coalescence of oil droplets, forming oil pockets, while hydrates detach from the oil droplets and flow suspended in the water phase. Hydrates suspended in water will result in the formation of porous structures that induce a higher local pressure loss. In the fourth stage, the system consists of an intermittent flow, formed by a region containing oil and another region containing mainly water and hydrates. Plugging eventually occurs when the local increase in pressure loss due to viscosity in the region of the flow containing the hydrates is high enough to stop the flow. Images from the camera, shown in the top panel of Figure 11, confirm the different stages until plugging. In the first one (left image), before hydrate formation, droplets have a regular shape. The second one is darker, after the onset of hydrate formation, as hydrates form around droplets. The last two, one on the right, show an intermittence, where one is dark because it is from a part of the flow that has hydrates, and the other one is transparent, from a part of the flow with only liquid, during oil-dominated flow.

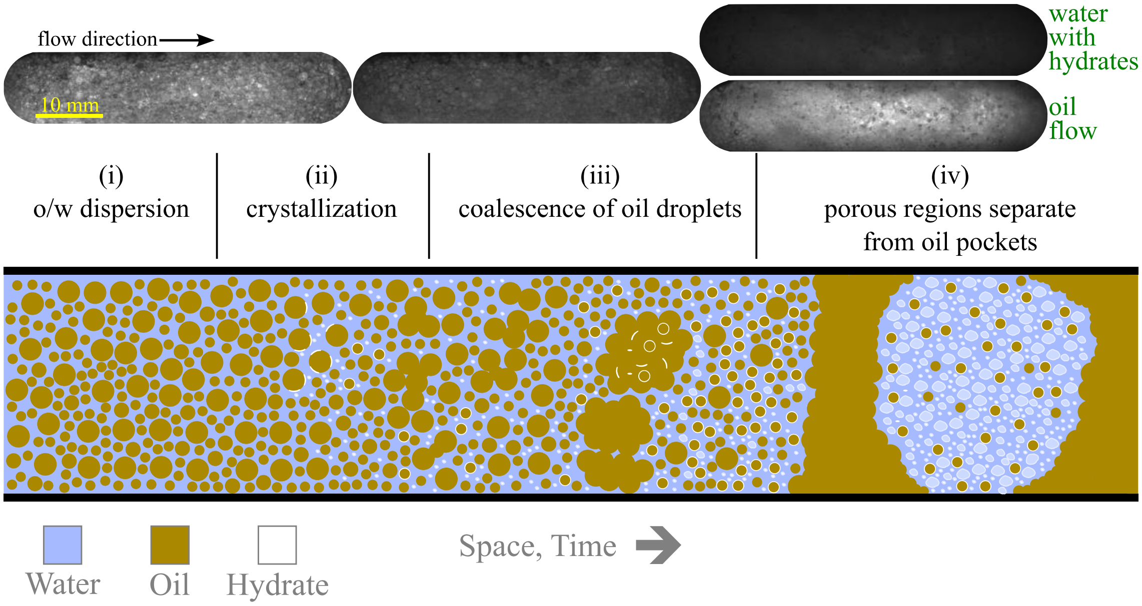

Figure 11. Depiction of the conceptual model for hydrate blockage at intermediate water cut.

4.4 Hydrate formation at high water cut

Figure 12 shows the time evolution of the dielectric together with density (panel (a)), dielectric with absolute energy (panel (b)), dielectric and chord counts (panel (c)), along with the time evolution of the horizontal pressure drop and flow rate (panel (d)) for a test at 80% water cut and 200 L/h. Hydrates formed after a few minutes, observed due to the gradual increase of absolute energy during the first ten minutes of experiments. After ten minutes, an important amount of hydrates is formed, enough to rapidly increase the chord counts (Figure 12(c)) detected in the FBRM range, which is 1-1000 µm. An oscillatory behavior is detected, for all the measurements, after 10 minutes, indicating that the flow is heterogeneous and, once again, parts of the flowing volume contain more hydrates than others: the transit of hydrates is therefore intermittent. Figure 12(a) shows that the density oscillates in a way that the troughs are around 950 kg/m^3, which can be a mixture of all the phases, while the crests are at more than 1000 kg/m^3, which means that there is mostly water on this part of the flow. Density and dielectric are in phase, as the time lag for a maximal Kendall correlation between the two data sets is 4 seconds. As a reminder, the tests are carried out with saline water, which has a density of more than 1000 kg/m^3, while hydrates have a density of around 910 kg/m^3 and oil has a density of around 815 kg/m^3. Therefore, with hydrates, the flow will be heterogeneous in the sense that there is a region that consists of water as a single phase and another region containing hydrates with oil flowing dispersed in the water continuous phase. Indeed, in Figure 12(b) one can notice that absolute energy and dielectric are in exact antiphase, i.e., the higher values of absolute energy (regions containing more hydrates) correspond to the troughs of dielectric (regions containing more oil).

The results shown in Figure 12(b) indicate that most of the hydrates entrap the oil phase, as evidence by the absolute energy being nearly 80 times higher when there is oil than when there is only water as a single phase. Although most of the hydrates flow entrapping oil droplets, it is expected that some hydrates may break apart from the oil droplets and flow suspended in the water continuous phase (de Almeida et al., 2022).

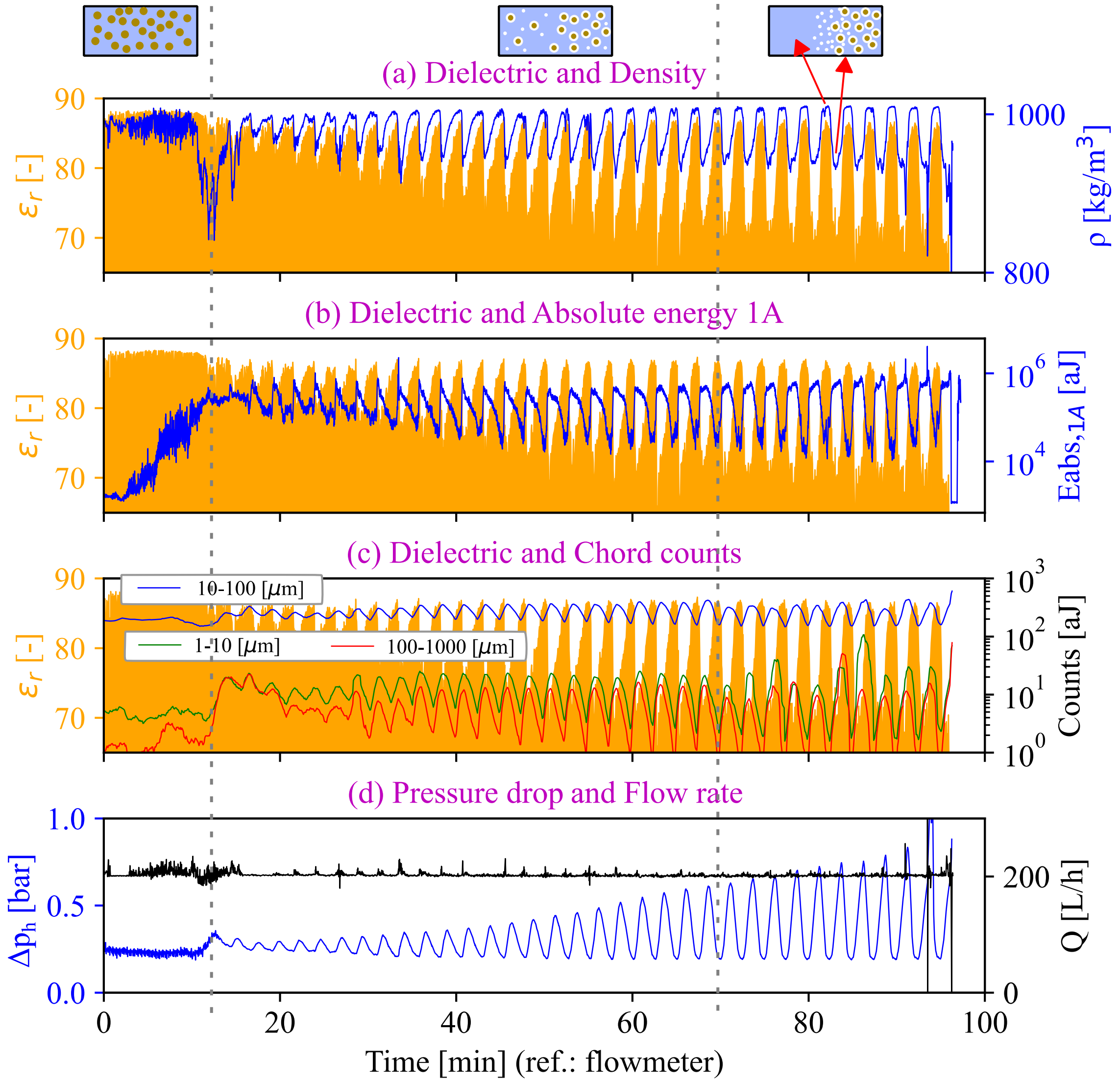

Figure 12. Experiment at 80% water-cut and 200 L/h (#12 in Table 5), showing the time evolution of (a) dielectric and density, (b) dielectric and absolute energy, (c) dielectric and chord counts, and (d) horizontal pressure drop and flow rate.

Using the method proposed in subsection 4.1 to calculate the time-lagged cross-correlation between density and absolute energy, for this test at 80% water cut, it is shown in Figure 13 that the time lag between the two data sets is about 1.3 minutes, which is approximately half of the period of oscillation of the curves. One can also notice that the lowest correlation occurs near the center, for a time lag of zero. This proves that the parts of the flow with more hydrates (peaks of absolute energy) are the same parts of the flow with more oil (valleys of density).

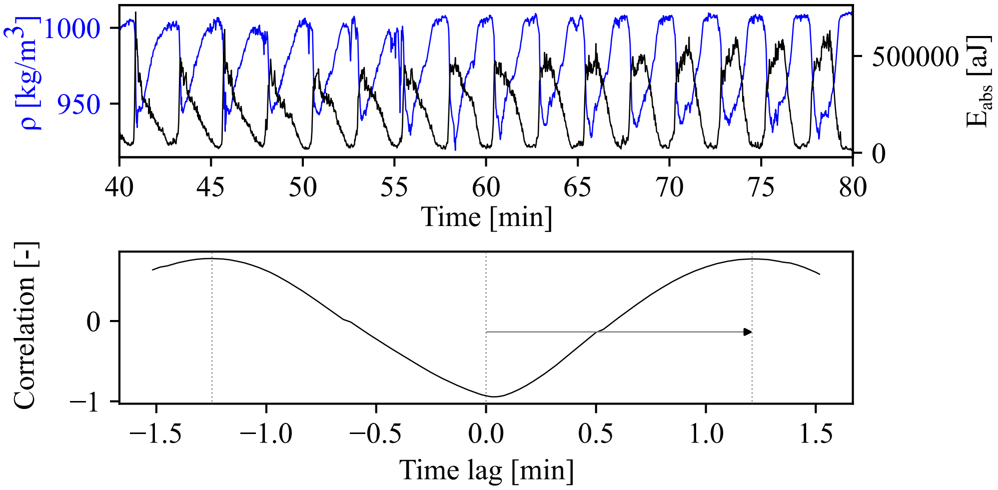

Figure 13. Time-lagged cross-correlation analysis between density and absolute energy for the test at 80% water cut (#12 in Table 5).

To gain better understanding of the formation of this oscillatory behavior, Figure 14 shows an enlarged portion of Figure 12(b,c) at two different moments: after a few minutes of hydrate formation (left panels), and close to the end of the experiment (right panels). By analyzing the absolute energy along with the chord counts, one notices a different pattern between the two cases. On the left, hydrates are mostly spread throughout the flow, with a front carrying more particles. In contrast, on the right panel, hydrates are mostly collected at the front, with dispersed hydrates that flow with the continuous phase, while part of the flow will contain mainly water without hydrates or dispersed oil droplets. This is likely due to the difference in velocity between suspended particles of different sizes. Smaller particles accumulate over time behind large hydrate particles because they are faster than the larger ones.

Figure 15 shows some images which visually confirm the intermittent behavior captured by the signals. The images on the left were taken during the passage of large agglomerates (the "front" part of the flow containing hydrates entrapping oil droplets), while images on the right are taken during the passage of parts of the flow containing mostly water as a single phase. The images observed on the right contain less and less hydrates over time, which corresponds to the reduction of absolute energy in that region of the flow (see Figure 14(b), between 86.5 and 87.5 minutes).

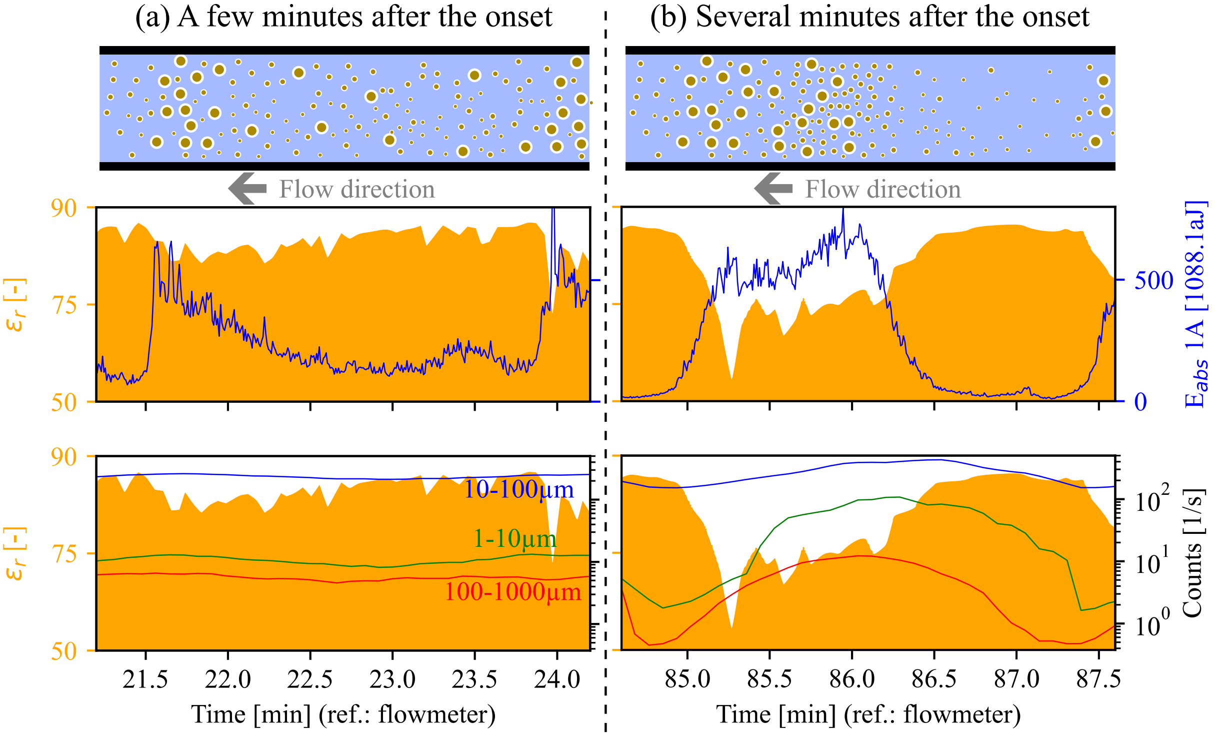

Figure 14. Comparison between dielectric, absolute energy and chord counts in two 3-minutes intervals for the experiment at 80% water cut and 200 L/h (#12 in Table 5).

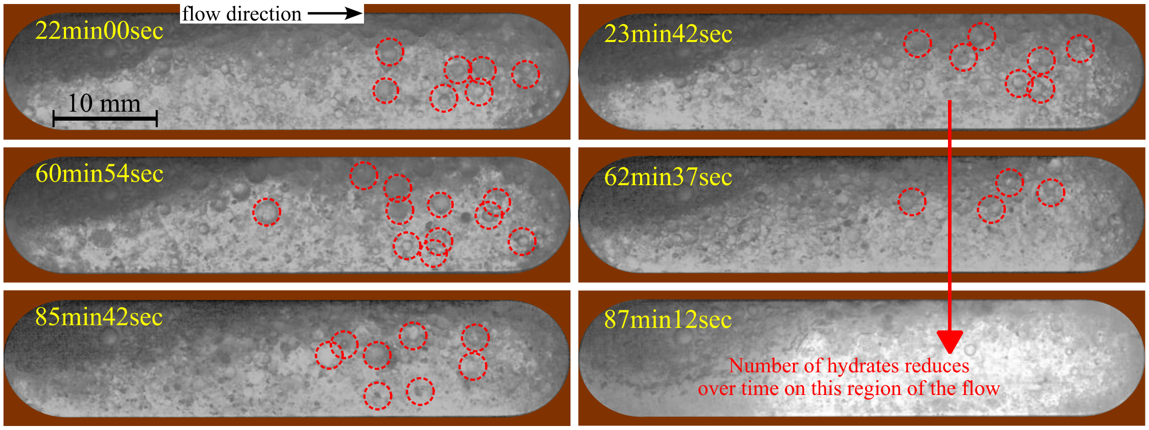

Figure 15. Images from the HSC for the experiment at 80% water cut and 200 L/h (#12 in Table 5) showing that parts of the flow contain hydrates all the time (images on the left), while others have a reduction in the number of particles over time (images on the right).

We conclude the section proposing a conceptual model for hydrate formation and plugging at high water cut in oil-water dispersed systems, based on our experiments at 80% water cut. The model, represented in Figure 16, contains four stages. The first stage is the formation of an oil-in-water dispersion due to the shear caused by the flow. The second step includes the onset of hydrate formation around oil droplets. Hydrates will trap the oil droplets, while part of the hydrates detaches from the oil surfaces and flow suspended in the water continuous phase. In the third stage, due to the difference in velocity between particles of different sizes, the flow gradually becomes heterogeneous. Small particles seem to accumulate more and more behind large particles, since they can flow faster than the large ones. In the fourth stage, as one region of the flow contains an important local hydrates fraction and has a high enough pressure loss due to viscosity, the plug may eventually occur. For this case, hydrate blockage is a gradual event, and it takes longer than for tests at intermediate or low water cut to occur.

In Figure 16, a few images from the camera are shown to illustrate how they compare to the different stages. The first image, on the left, shows the flow before hydrate formation. The second image was taken at the early stages of hydrate formation, when the droplets become darker, as hydrates form around them. The two images on the right are from the two different structures during the last stage, when one part of the flow contains hydrates entrapping oil suspended in water and the other part contains mostly water.

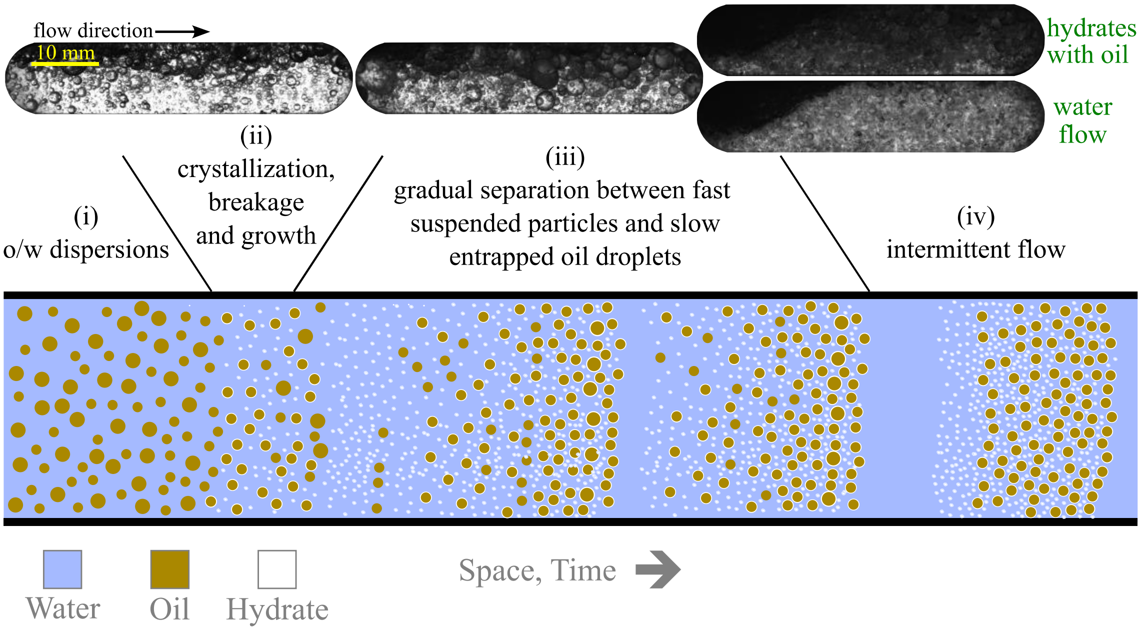

Figure 16. Depiction of the conceptual model for hydrate blockage at high water cut.

4.5 Estimating the local hydrate fraction

It was concluded in previous sections that hydrates are not evenly distributed in the flow. In fact, some parts of the flow contain more hydrates than others, and this uneven distribution is an important cause of plugging. Knowledge of the local hydrate fraction is essential to identify why the plugging occurs, which is necessary for the development of strategies aimed at limiting the risk of plugging. For this, in this subsection, it is proposed a simplified model based on the density measurement obtained from the Coriolis flowmeter to estimate the local fraction of each phase ($\alpha_{l,O}$ for oil, $\alpha_{l,W}$ for water, and $\alpha_{l,H}$ for hydrate) flowing in the loop.

The density measured by the Coriolis is influenced by the densities of the three phases that flow in the pipeline (water, hydrates and oil). This can be mathematically expressed as:

$$\rho = \rho_H \alpha_{l,H} + \rho_W \alpha_{l,W} + \rho_O \alpha_{l,O} \tag{10}$$

It was explained in previous sections that hydrates are transported preferentially by the water phase at low and intermediate water cut, or preferentially by the oil phase at high water cut. In this sense, it is assumed that the proportion of local fraction of hydrates relative to the carrier phase is uniform in space and equal to the global proportion of those phases in volume. In other words, locally in the flow, the quantity of hydrates relative to the phase that transports the hydrates is everywhere the same.

Therefore, if hydrates are transported by the water phase, it is assumed that, at any given instant, the local fraction of hydrates is proportional to the local water fraction via the global hydrate-to-water volume fraction:

$$\frac{\alpha_{l,H}}{\alpha_{l,W}} = \frac{V_H}{V_W} \tag{11}$$

However, if hydrates are preferentially transported by the oil phase, it is assumed that, at any given time, the local hydrate fraction is proportional to the local oil fraction via the global hydrate-to-oil volume fraction:

$$\frac{\alpha_{l,H}}{\alpha_{l,O}} = \frac{V_H}{V_O} \tag{12}$$

It should be noted that the volumes of the three phases (V_W, V_O, V_H) are time-dependent and must be calculated in advance using the model proposed in section 3. Finally, the sum of all phases results in the simple relation:

$$\alpha_{l,H} + \alpha_{l,W} + \alpha_{l,O} = 1 \tag{13}$$

The model represented by equations (10)-(13) can be used to calculate the local fractions that pass through the Coriolis flowmeter. At low water cut, as illustrated in Figure 8 and Figure 11, where hydrates are transported by the water phase, equations (10), (11) and (13) are used. By combining these equations, the following expression can deduced for the local hydrate fraction:

$$\alpha_{l,H} = \frac{\rho - \rho_O}{\rho_H - \rho_O + (\rho_W - \rho_O)\frac{V_W}{V_H}} \qquad (14)$$

At high water cut, as illustrated in Figure 16, where hydrates flow preferably with the oil phase, it is used equations (11), (12) and (13), from which the following expression is deduced:

$$\alpha_{l,H} = \frac{\rho - \rho_W}{\rho_H - \rho_W + (\rho_O - \rho_W)\frac{V_O}{V_H}} \qquad (15)$$

Figure 17 shows the application of equation (14) for a test at 30% water cut and 200 L/h (#1 in Table 5). The hydrate fraction and local hydrate fraction are shown in Figure 17(a), while the absolute energy from sensor 1A is shown in Figure 17(b). The peaks observed in the local hydrate fraction are in phase with the peaks observed in the absolute energy, which indicates that the model is accurately capturing the regions containing more hydrates and regions with more liquid. Despite the final global hydrate fraction in the whole system (in orange) being nearly 7%, the local hydrate fraction can vary between 0 and approximately 18%. It is also important to consider that, due to the porosity, water is trapped inside the hydrate particles and, therefore, the volume fractions of the structures containing hydrates and water (see Figure 8) are expected to be much larger than the calculated local hydrate fractions.

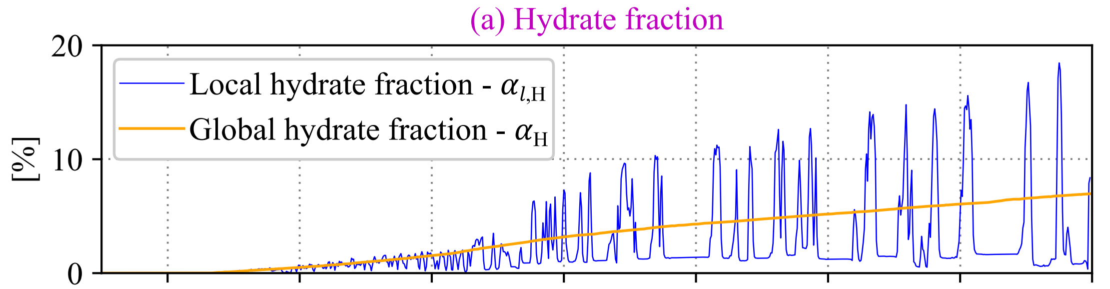
(a) Hydrate fraction

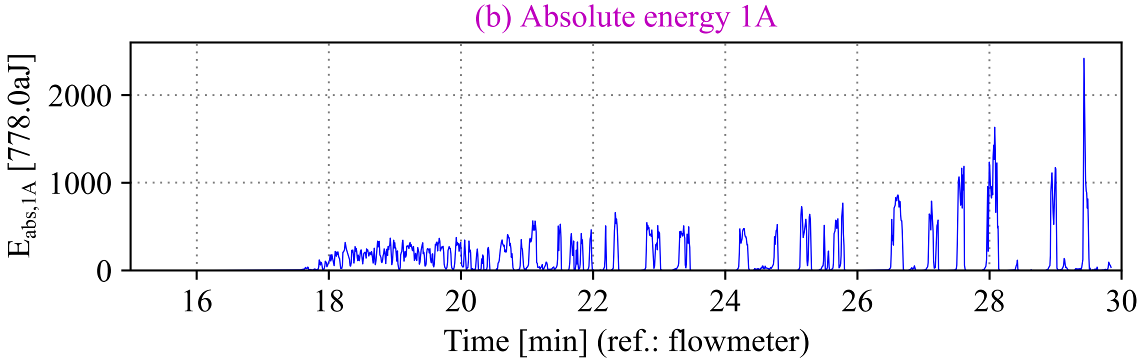
(b) Absolute energy 1A

Figure 17. Hydrate fractions and absolute energy for a test at 30% water-cut and 200 L/h (#1 in Table 5).

Figure 18 shows hydrate fraction, local hydrate fraction and absolute energy for a test at 50% water cut and 400 L/h (#9 in Table 5). The global hydrate fraction in the system just before plugging (orange line, top panel) is approximately 6.6%, but due to the heterogeneous suspension of hydrates and their accumulation in some parts of the liquid, the local hydrate fraction (blue line, top panel) that passes through the Coriolis varies between 0 and 11.3%. Once more, the peaks of the local hydrate fraction are in phase with the peaks of absolute energy (bottom panel).

(a) Hydrate fraction

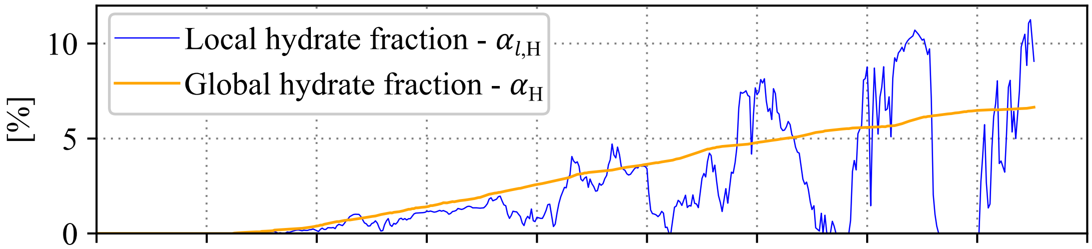

(b) Absolute energy 2A

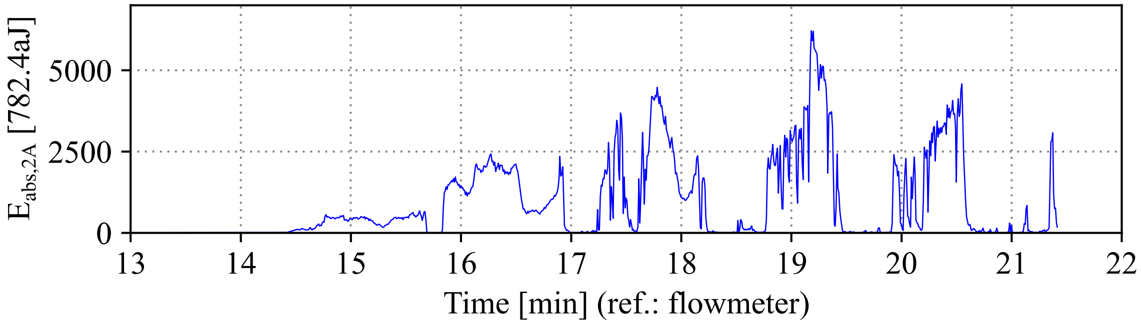

Figure 18. Local hydrate fraction and absolute energy for a test at 50% water-cut and 400 L/h (#9 in Table 5).

The application of equation (15) for a test at 80% water cut and 200 L/h (#12 in Table 5) is shown in Figure 19. The hydrate fraction (orange line, top panel) is approximately 8.5% just before plugging, but due to the heterogeneity of the flow, the local hydrate fraction may be up to 13.3%. One can notice that the peaks observed for local hydrate fraction are in phase with the absolute energy (bottom panel).

The proposed model can be used to predict plugging by monitoring local peaks of the hydrate fraction. However, it is important to discuss the limitations of the model that led to the development of equations (14) and (15). It can only be used when all the hydrates are being transported by one phase only, water or oil. In this sense, further experiments combined with the implementation of other techniques to obtain the local hydrate fraction could validate the proposed model. Despite its limitations, equations (14) and (15) can be used for a rapid estimation of the local hydrate in the system and help to better understand the degree of heterogeneity of the flow.

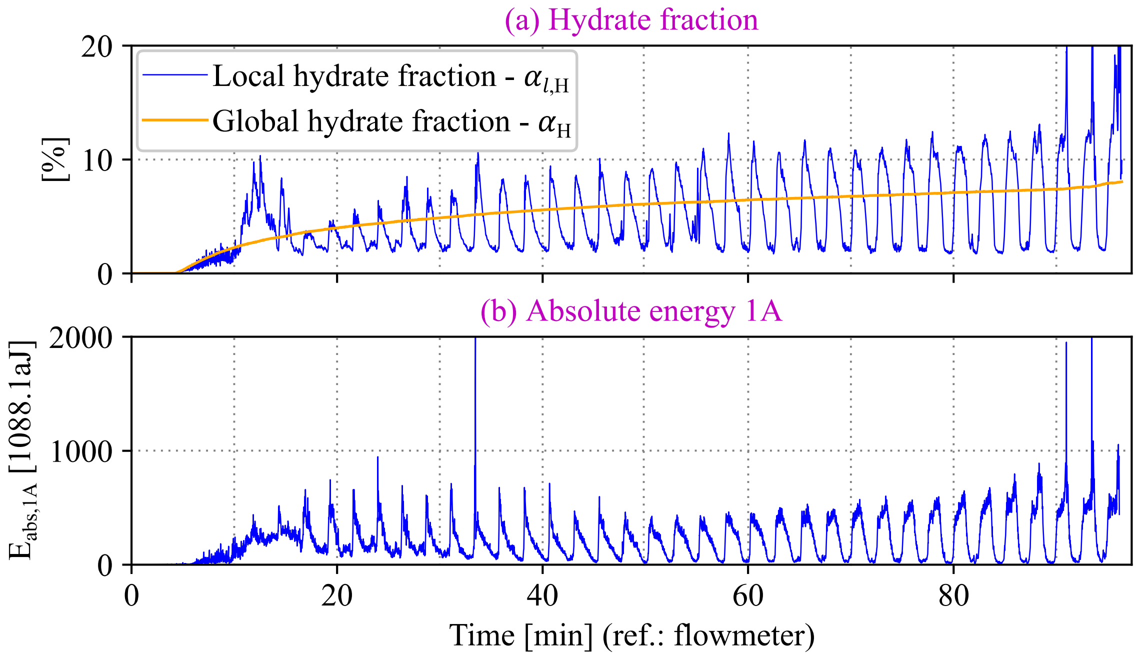

Figure 19. Apparent hydrate fraction and absolute energy for a test at 80% water-cut and 200 L/h (#12 in Table 5).

To conclude the analysis, a methodology to classify the tests according to their heterogeneity is proposed here. It consists of calculating the volume fraction of the flow (relative to the global volume of liquid and hydrates inside the flow loop) that contains 50% of all the hydrates (the upper half of data) formed globally in the system. This means that an integration of the local hydrate fraction (equations (14) or (15)) over time is performed during the last lap around the loop, just before plugging, in a decrescent order from the highest to the lowest hydrate fraction, while keeping track of the volume as a function of the flow rate measured by the Coriolis. For instance, a system that is highly heterogeneous will have 50% of the hydrates accumulated in a very small fraction of the flow.

This method is applied to all the tests listed in Table 5. The results are shown in Figure 20, which shows the time for plugging since the onset of hydrate formation as a function of the volume (in fraction) occupied by the 50% of the hydrates (the upper half of data) flowing in the pipeline.

The results indicate that tests at high water cut (in red) are less prone to plug and are more homogeneous, with 50% of the hydrates concentrated in a volume fraction between 26% and 34% of the flow volume. As the water cut reduces, the slurry flow regime becomes increasingly heterogeneous and plugs faster than at high water cut. For the tests at intermediate water cut (in blue), hydrates are concentrated in a volume fraction between 17% and 28% of the volume, while for tests at low water cut, they are concentrated in a volume fraction between 10% and 23%.

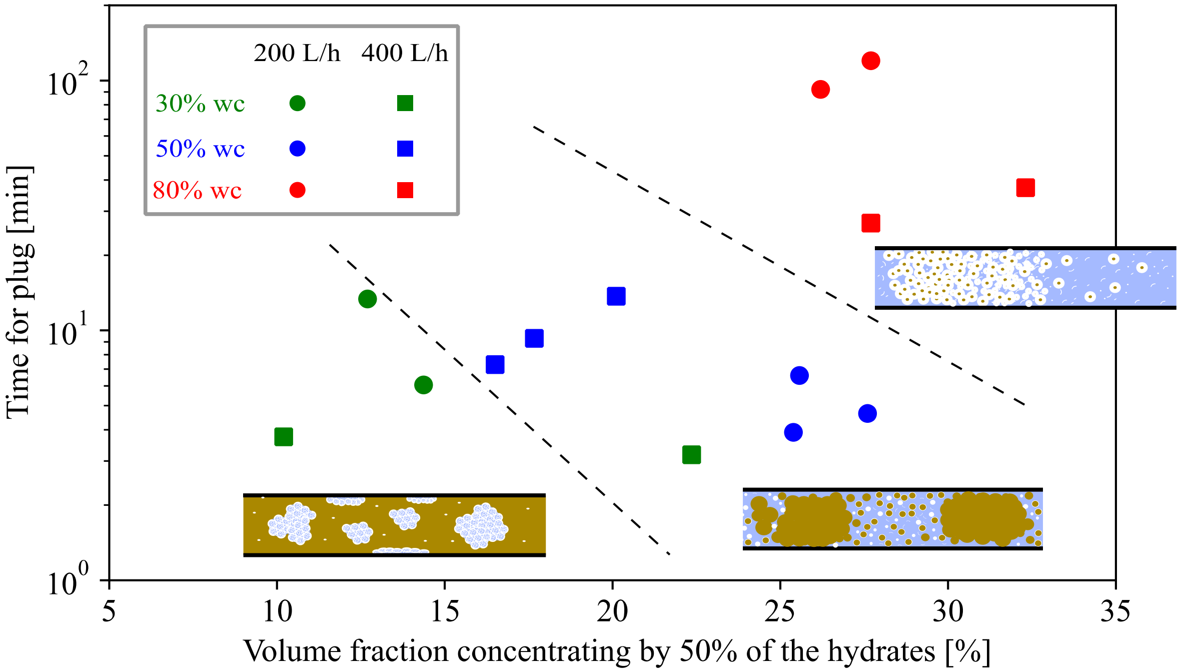

Figure 20. Time for plugging as a function of the heterogeneity of the system.

4.6 Summary of results

As previously discussed, from the literature, the conceptual models of hydrate formation and plugging in oil-water dispersed systems assume that the formation of large particles that cause plugging occurs mainly due to agglomeration. Agglomeration models have been extensively studied. In this work, it was observed, however, that there are other mechanisms that deserve better attention and could be very important for a better understanding of how plugging occurs.

Separation of phases has been observed in the tests, whose main outcomes are summarized in Table 6. The separation of phases changes the flow regime in a way that presents distinct structures along space, comparable to an intermittent flow. Parts of the flowing volume have higher concentrations of hydrates than others. This can be because structures of different sizes or densities will flow at different velocities, which facilitates the formation of the intermittent flow. It was also observed, especially at low and intermediate water cut, that the dispersed phase rapidly coalesces (large water pockets at low water cut, or large oil pockets at intermediate water cut). This mechanism is not well understood and requires additional studies. The analysis proposed in section 4.5 showed that this separation of phases is more significant at low and intermediate water cut, and it can lead to plugging in a few minutes.

Table 6. Summary of conceptual mechanisms for hydrate blockage from low to high water cuts.

Water cut	**Model**
Low	A water-in-oil dispersion is the initial flow regime. When hydrates form, they break into water droplets. Water droplets coalesce, forming large pockets of water with suspended hydrates. Deposition occurs, and hydrates become highly concentrated in a portion of the flowing volume, which eventually causes plugging.
Intermediate	An oil-in-water dispersion is the flow regime in the beginning. When hydrates form, they preferably break into the water phase, while oil droplets coalesce. This leads to deposition and concentration of hydrates in parts of the flow, eventually causing plugging.
High	An oil-in-water dispersion is the initial flow regime. Hydrates initially form around oil droplets. As they continue forming and entrapping the oil droplets, part of them breaks into the water continuous phase. Suspended particles seem to flow faster than hydrates with entrapped oil, resulting in a gradual transition to an intermittent flow.

5 Conclusions

In this work, flow loop tests were carried out with hydrate formation in oil-water flow at 30%, 50% and 80% water cut. New mechanisms on how the slurry flow after hydrate formation is and how hydrate blockage occurs were proposed. The main conclusion from the experiments is that there is a formation of a heterogeneous flow that results from a separation of phases. The resulting flow patterns are characterized by parts of the flow containing more hydrates than others. Deposition was also an important mechanism that contributed to plugging formation.

At low water cut, hydrate formation completely modifies from the initial water-in-oil dispersion to a flow pattern composed of large water pockets with hydrates that rapidly plug the system. At intermediate water cut, a rapid separation of phases is observed, disrupting the oil-in-water dispersion and forming a flow with a pattern composed of two main structures: one being a large pocket of oil, and another region containing hydrates suspended in the water phase. At high water-cut, hydrates apparently entrap the oil phase, as it was shown that hydrates flow mostly with the oil phase, although part of the hydrates may break loose and become suspended in the water continuous phase.

A simplified model based on density measurement was proposed to estimate the local hydrate fraction and quantify the heterogeneity of the system. It was shown that tests at high water cut are less heterogeneous, which explains why they flow much longer than at intermediate or low water cut. The extension of the tests to other conditions, the improvement and validation of the model could be conducted in a further work for a better understanding of the mechanism of plugging due to the formation of these heterogeneous flows and the quantification of the transportability of the system.

ACKNOWLEDGMENTS

The authors would like to acknowledge the financial support from TotalEnergies in the framework of the Archimede 5 project. We would like to thank the technical support provided by the staff of Mines Saint-Etienne. We also thank Mr. P. Glénat, who recently retired from TotalEnergies, for sharing his valuable experience and knowledge, which greatly contributed to the development of this work.

REFERENCES

Bassani, C.L., Barbuto, F.A.A., Sum, A.K., Morales, R.E.M., 2017. Modeling the effects of hydrate wall deposition on slug flow hydrodynamics and heat transfer. Appl Therm Eng 114, 245–254. https://doi.org/10.1016/j.applthermaleng.2016.11.175

Bassani, C.L., Melchuna, A.M., Cameirão, A., Herri, J.M., Morales, R.E.M., Sum, A.K., 2019. A multiscale approach for gas hydrates considering structure, agglomeration, and transportability under multiphase flow conditions: I. phenomenological model. Ind Eng Chem Res 58, 14446–14461. https://doi.org/10.1021/acs.iecr.9b01841

Cardoso, C.A.B.R., Gonçalves, M.A.L., Camargo, R.M.T., 2015. Design options for avoiding hydrates in deep offshore production. J Chem Eng Data 60, 330–335. https://doi.org/10.1021/je500601f

Chen, J., Liu, J., Chen, G.J., Sun, C.Y., Jia, M.L., Liu, B., Si, S., Ren, N., 2014. Insights into methane hydrate formation, agglomeration, and dissociation in water + diesel oil dispersed system. Energy Convers Manag 86, 886–891. https://doi.org/10.1016/j.enconman.2014.06.056

Chen, L., Koh, C.A., Sun, B., 2022. Insight into the plugging mechanism in water-continuous hydrate slurries. Fuel 316. https://doi.org/10.1016/j.fuel.2022.123360

Cheong, J.H., 2020. Four ways to quantify synchrony between time series data. https://doi.org/10.17605/OSF.IO/BA3NY

Colombel, E., Gateau, P., Barré, L., Gruy, F., Palermo, T., 2009. Discussion of Agglomeration Mechanisms between Hydrate Particles in Water in Oil Emulsions. Oil and Gas Science and Technology 64, 629–636. https://doi.org/10.2516/ogst/2009042

de Almeida, V., Serris, E., Cameirão, A., Herri, J.-M., Abadie, E., Glénat, P., 2022. Monitoring gas hydrates under multiphase flow in a high pressure flow loop by means of an acoustic emission technology. J Nat Gas Sci Eng 97, 104338. https://doi.org/10.1016/j.jngse.2021.104338

Delahaye, A., Fournaison, L., Marinhas, S., Martínez, M.C., 2008. Rheological study of CO2 hydrate slurry in a dynamic loop applied to secondary refrigeration. Chem Eng Sci 63, 3551–3559. https://doi.org/10.1016/j.ces.2008.04.001

Ding, L., Shi, B., Liu, Y., Song, S., Wang, W., Wu, H., Gong, J., 2019. Rheology of natural gas hydrate slurry: Effect of hydrate agglomeration and deposition. Fuel 239, 126–137. https://doi.org/10.1016/j.fuel.2018.10.110

Ding, L., Shi, B., Lv, X., Liu, Y., Wu, H., Wang, W., Gong, J., 2016. Investigation of natural gas hydrate slurry flow properties and flow patterns using a high pressure flow loop. Chem Eng Sci 146, 199–206. https://doi.org/10.1016/j.ces.2016.02.040

Englezos, P., 1993. REVIEWS Clathrate Hydrates, Ind. Eng. Chem. Res.

Fidel-Dufour, A., Gruy, F., Herri, J.M., 2006. Rheology of methane hydrate slurries during their crystallization in a water in dodecane emulsion under flowing. Chem Eng Sci 61, 505–515. https://doi.org/10.1016/j.ces.2005.07.001

Jamaluddin, A.K.M., Kalogerakis, N., Bishnoi, P.R., 1991. Hydrate plugging problems in undersea natural gas pipelines under shutdown conditions.

Khurana, M., Yin, Z., Linga, P., 2017. A review of clathrate hydrate nucleation. ACS Sustain Chem Eng. https://doi.org/10.1021/acssuschemeng.7b03238

Liu, Z., Vasheghani Farahani, M., Yang, M., Li, X., Zhao, J., Song, Y., Yang, J., 2020. Hydrate slurry flow characteristics influenced by formation, agglomeration and deposition in a fully visual flow loop. Fuel 277. https://doi.org/10.1016/j.fuel.2020.118066

Melchuna, A., Cameirão, A., Herri, J.M., Glénat, P., 2016. Topological modeling of methane hydrate crystallization from low to high water cut emulsion systems. Fluid Phase Equilib 413, 158–169. https://doi.org/10.1016/j.fluid.2015.11.023

Olajire, A.A., 2020. Flow assurance issues in deep-water gas well testing and mitigation strategies with respect to gas hydrates deposition in flowlines - A review. J Mol Liq. https://doi.org/10.1016/j.molliq.2020.114203

Pham, T.K., Cameirão, A., Melchuna, A., Herri, J.M., Glénat, P., 2020. Relative pressure drop model for hydrate formation and transportability in flowlines in high water cut systems. Energies (Basel) 13. https://doi.org/10.3390/en13030686

Schober, P., Schwarte, L.A., 2018. Correlation coefficients: Appropriate use and interpretation. Anesth Analg 126, 1763–1768. https://doi.org/10.1213/ANE.0000000000002864

Shaibu, R., Sambo, C., Guo, B., Dudun, A., 2021. An assessment of methane gas production from natural gas hydrates: Challenges, technology and market outlook. Advances in Geo-Energy Research. https://doi.org/10.46690/ager.2021.03.07

Sinquin, A., Palermo, T., Peysson, Y., 2004. Rheological and Flow Properties of Gas Hydrate Suspensions, Oil & Gas Science and Technology-Rev. IFP. https://doi.org/10.2516/ogst:2004005

Sloan, D., Koh, C., Sum, A.K., 2011. Natural Gas Hydrates in Flow Assurance. Gulf Professional Printing. https://doi.org/10.1016/C2009-0-62311-4

Sloan, E.D., 2003. Fundamental principles and applications of natural gas hydrates. Nature 426, 353–359.

Sloan, E.D., Koh, C.A., 2008. Clathrate Hydrates of Natural Gases, Third Edition. ed. CRC Press.

Song, G.C., Li, Y.X., Wang, W.C., Liu, S., Wang, X.Y., Shi, Z.Z., Yao, S., 2019. Experimental investigation on the microprocess of hydrate particle agglomeration using a high-speed camera. Fuel 237, 475–485. https://doi.org/10.1016/j.fuel.2018.09.155

Stoner, H.M., Koh, C.A., 2021. Perspective on the role of particle size measurements in gas hydrate agglomeration predictions. Fuel. https://doi.org/10.1016/j.fuel.2021.121385

Straume, E.O., Kakitani, C., Merino-Garcia, D., Morales, R.E.M., Sum, A.K., 2016. Experimental study of the formation and deposition of gas hydrates in non-emulsifying oil and condensate systems. Chem Eng Sci 155, 111–126. https://doi.org/10.1016/j.ces.2016.07.046

Sum, A.K., Koh, C.A., Sloan, E.D., 2009. Clathrate hydrates: From laboratory science to engineering practice. Ind Eng Chem Res. https://doi.org/10.1021/ie900679m

Turner, D.J., 2005. Clathrate Hydrate Formation in Water-in-oil Dispersions. Golden.

Wang, Z., Tong, S., Wang, C., Zhang, J., Fu, W., Sun, B., 2020. Hydrate deposition prediction model for deep-water gas wells under shut-in conditions. Fuel 275. https://doi.org/10.1016/j.fuel.2020.117944